

Microglial activation, recruitment and phagocytosis as linked phenomena in ferric oxide nanoparticle exposure

Yun Wang^{a,b,1}, Bing Wang^{a,1}, Mo-Tao Zhu^a, Ming Li^a, Hua-Jian Wang^a, Meng Wang^a, Hong Ouyang^a, Zhi-Fang Chai^a, Wei-Yue Feng^{a,*}, Yu-Liang Zhao^a

^a Key Laboratory for Biomedical Effects of Nanomaterials and Nanosafety and Key Laboratory of Nuclear Analytical Techniques, Institute of High Energy Physics, Chinese Academy of Sciences, Beijing 100049, China

^b Department of Occupational and Environmental Health Sciences, School of Public Health, Peking University, Beijing 100191, China

ARTICLE INFO

Article history:

Received 23 March 2011

Received in revised form 29 April 2011

Accepted 1 May 2011

Available online 7 May 2011

Keywords:

Ferric oxide nanoparticles

Neurotoxicity

Microglial activation

ABSTRACT

Microglia as the resident macrophage-like cells in the central nervous system (CNS) play a pivotal role in the innate immune responses of CNS. Understanding the reactions of microglia cells to nanoparticle exposure is important in the exploration of neurobiology of nanoparticles. Here we provide a systemic mapping of microglia and the corresponding pathological changes in olfactory-transport related brain areas of mice with Fe₂O₃-nanoparticle intranasal treatment. We showed that intranasal exposure of Fe₂O₃ nanoparticle could lead to pathological alteration in olfactory bulb, hippocampus and striatum, and caused microglial proliferation, activation and recruitment in these areas, especially in olfactory bulb. Further experiments with BV2 microglial cells showed the exposure to Fe₂O₃ nanoparticles could induce cells proliferation, phagocytosis and generation of ROS and NO, but did not cause significant release of inflammatory factors, including IL-1β, IL-6 and TNF-α. Our results indicate that microglial activation may act as an alarm and defense system in the processes of the exogenous nanoparticles invading and storage in brain.

© 2011 Elsevier Ireland Ltd. All rights reserved.

1. Introduction

Over the past few years, the safety of nanomaterials has attracted much attention because the rapid development of nanotechnology induce the quite possibilities that more and more nanomaterials are moving from research benches to the manufacturing lines, and thus come into people's life, whereas, in the mean time, their potential adverse impact on human health is still far from known. Up to now, nanomaterials have been shown to enter human body via inhalation, ingestion, dermal penetration, or injection (Oberdörster et al., 2005; Stern and McNeil, 2008). The small size of nanoparticles (NPs) facilitates the uptake of particles into cells and transport into blood and lymph circulation to reach potentially sensitive target sites (Kreyling et al., 2002). Several studies indicate that nano-sized particles can cross the blood–brain barrier and enter the central nervous system (CNS) of animals (Elder et al., 2006; Lockman et al., 2003). Besides, the olfactory nerve path-

way should be considered as a portal of entry of nanoparticles into the CNS under conditions of airborne nanoparticle exposure (Oberdörster et al., 2004; Elder et al., 2006). So far, many kinds of nanoparticles, such as gold (De Lorenzo and Darin, 1970), elemental ¹³C (Oberdörster et al., 2004), manganese oxide (Elder et al., 2006), titanium dioxide (Wang et al., 2008b) and ferric oxide NPs (Wang et al., 2007, 2009) have all been demonstrated to transport into CNS via the olfactory pathway in animals. The CNS as an importantly potential target organ attracts deep concern about the toxicological effects of nanoparticles (Sharma, 2007; Suh et al., 2009). However, little is known about the interactions between nanoparticles and CNS.

It is generally known that the immune system protects the body against invasion by any foreign microorganism. The CNS because of its unique anatomy and physiology has an immune system of its own, which is comprised of microglia (Block et al., 2007). Microglia are the resident macrophage-like cells of the brain and spinal cord. Under normal conditions, the number of microglia is limited, constituting 20% of the total glial cell population within the brain and are characterized by a small cell body with fine, ramified processes and low expression of surface antigens (Hanisch and Kettenmann, 2007; Graeber, 2010). When the CNS is injured, microglia may migrate to the damaged sites and become activated accompanying with rapidly transform their morphology, proliferate and enhance antigen presentation (Graeber,

* Corresponding author at: CAS Key Laboratory for Biomedical Effects of Nanomaterials and Nanosafety and CAS Key Laboratory of Nuclear Analytical Techniques, Institute of High Energy Physics, Chinese Academy of Sciences, P.O. Box 918, Beijing 100049, China. Tel.: +86 10 88233209; fax: +86 10 88235294.

E-mail address: fengwy@mail.ihep.ac.cn (W.-Y. Feng).

¹ These authors contributed equally to this work.

2010; Luo et al., 2010). Activated microglia can promote both protective and harmful effects. Beneficial effects include removal of cell debris and myelin fragments, buffering of toxic compounds, and secretion of neurotrophins and cytokines to repair the injured neurons (Graeber, 2010; Block et al., 2007). However, the over-activated microglia can release a large array of cytotoxic factors, including tumor necrosis factor- α (TNF- α), 1L-1 β , 1L-6 and so forth, and free radicals, such as reactive oxygen species (ROS) and nitric oxide (NO), which has been implicated in the pathogenesis of numerous neurodegenerative diseases, such as Alzheimer's disease, Parkinson's disease, multiple sclerosis, viral infections, HIV dementia and so forth (Block et al., 2007; Graeber, 2010; Luo et al., 2010).

Our previous work showed some evidence that the intranasally stored Fe₂O₃ NPs could transport into the brain via olfactory route and induce oxidative stress and nerve cell damage in mouse brain (Wang et al., 2007, 2009). In this study by using immunofluorescence technique, the confocal images showed the microglia was activated by their morphology transforming and proliferating in olfactory bulb, hippocampus and striatum after Fe₂O₃ NP intranasal exposure. The recruitment of microglia was in consistent with the pathway of Fe₂O₃ NP transportation in the brain that determined by synchrotron radiation X-ray fluorescence (SR-XRF). Experiments using microglial cells (BV2) confirmed the exposure of Fe₂O₃ NPs could induce significant release of intracellular ROS and NO. The nanoparticles were found to be phagocytized into microglial cells and localized in vesicles by transmission electron microscopy (TEM) images. These results will be helpful to further understand the interactions of nanoparticles with brain and thus be beneficial for the proper application of nanomaterials in biomedicine.

2. Materials and methods

2.1. Characterization of Fe₂O₃ nanoparticles

Two types of ferric oxide nanoparticles including α -Fe₂O₃ and γ -Fe₂O₃ NPs were used in the experiments. The α -Fe₂O₃ NPs were purchased from Nanjing Haitai Nanomaterial Co. Ltd., China. The γ -Fe₂O₃ NPs were purchased from Sigma–Aldrich Inc., USA. The size of the particles was characterized by TEM (JEOL JEM-200CX). Crystalline phase was identified by X-ray powder diffractometry (XRD, X'Pert PRO, X'Celerator). The specific surface area (SSA) of the particles was measured according to Brunauer–Emmett–Teller (BET) method (Quantachrome, Autosorb 1, Boynton, FL, USA). The magnetic property was determined using a vibrating sample magnetometer (VSM, LDJ9600, USA).

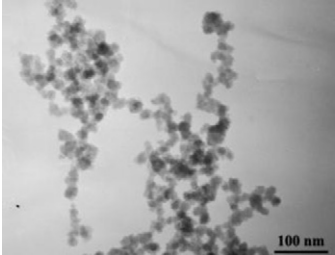
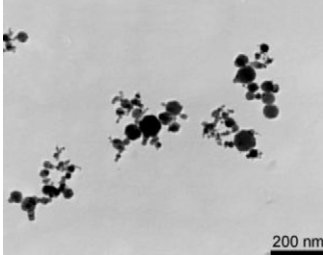
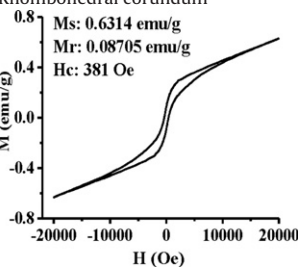
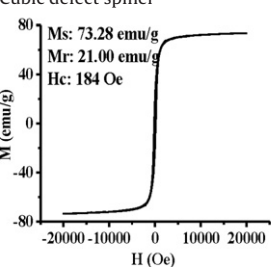
The particle sizes in calcium- and magnesium-free phosphate-buffered saline (PBS) and cell culture medium (Dulbecco's Modified Eagle Medium, DMEM) were measured. Briefly, the α -Fe₂O₃ and γ -Fe₂O₃ NPs were dispersed in PBS or cell culture medium at final iron concentration of 0.02, 0.2 and 2 mmol/L. The suspensions were supersonicated for 20 min to break up aggregates. The particle hydrodynamic diameters were tested by dynamic light scattering (DLS) measurements (90Plus Particle Size Analyzer, Brookhaven Instrument Corp., USA). The Zeta potentials (Delsa 440SX Zeta potential Analyzer, Beckman-Coulter, Fullerton, USA) of the particles were determined to identify the stability of the suspensions.

2.2. Animal and experimental design

The healthy CD-1CR male mice of 4-week-old and 20–22 g body weight were supplied by the Department of Laboratory Animal Science, Peking University Health Center. The mice were fed a commercial pellet diet and deionized water *ad libitum*, and kept in plastic cages in a 20 \pm 2 °C and 50–70% relative humidity room with a 12 h light/dark cycle. After one week accommodation, twenty mice were randomly divided into four groups: control, lipopolysaccharide (LPS), α -Fe₂O₃ and γ -Fe₂O₃ NP groups. The animal experiments were carried out in accordance with the Guiding Principles in the Use of Animals in Toxicology adopted by Society of Toxicology.

The Fe₂O₃ NPs were dispersed in physiological saline solution containing 0.1% sodium carboxy methyl cellulose (SCMC) and ultrasonic vibrated for 5 min. In order to obtain homogenized suspension, the particle dispersion solution was stirred on vortex agitator before every use. The instilled dose was selected based on the permis-

Table 1
Physicochemical properties of ferric oxide nanoparticles.

Nanoparticles	α -Fe ₂ O ₃ NPs	γ -Fe ₂ O ₃ NPs
Shape: TEM image		
Diameter	(22 \pm 5) nm	(31 \pm 17) nm
Specific surface area	11.18 m ² /g	33.21 m ² /g
Crystal structure	Rhombohedral corundum	Cubic defect spinel
Magnetic hysteresis loop		
Hydrodynamic diameter		
in PBS	794.3 nm	2732 nm
in DMEM	1546 nm	3128 nm
in DMEM with 10% FCS	143 nm	644 nm
Zeta potential		
in DMEM	−10.5 mv	−5.3 mv
in DMEM with 10% FCS	−12.5 mv	−13 mv

Note: The particle hydrodynamic diameters and zeta potential was tested in the iron concentrations of 2 mmol/L. Ms: saturated magnetization, Mr: remanent magnetization, Hc: coercive force.

sible exposure limit (PEL) for iron oxide fume (10 mg/m^3 for 8 h/day exposure) set by Occupational Safety and Health Administration (OSHA, 2003). The total permissible dose of Fe_2O_3 nanoparticle for a 20-g-weight mouse was calculated as 1.31 mg/day . In this study, a total amount of $130 \text{ }\mu\text{g}$ of $\alpha\text{-Fe}_2\text{O}_3$ or $\gamma\text{-Fe}_2\text{O}_3$ NPs (6.5 g/L , $10 \text{ }\mu\text{L}$ per nostril), which was ten times lower than the permissible inhalation dose for mouse, were intranasally instilled every other day into two nostrils of the mice for a period of 40 days. The control mice were instilled with 0.1% SCMC physiological saline solution instead ($10 \text{ }\mu\text{L}$ per nostril). The LPS group mice (used as positive control) were *i.p* injected with 5 mg/kg LPS (*Escherichia coli* 055:B5, Sigma–Aldrich Inc., USA) 3 h before sacrifice. During the experiments, no significant changes in the body weight of the exposed mice were found (Supplemental Data, Table S1).

2.3. Micro-distribution assay of iron in brain regions by SR- μXRF

The micro-distribution mapping of iron in the rat brain after nanoparticle intranasal exposure was achieved by synchrotron radiation micro-beam X-ray fluorescence (SR- μXRF). The SR- μXRF experiment (2.5 GeV , maximum current of 250 mA) was performed at the Beijing Synchrotron Radiation Facility (BSRF) 3W1A beamline, with space resolution of several micrometer and detection limit of ng/g range. The incident beam was focused approximately $20 \text{ }\mu\text{m} \times 30 \text{ }\mu\text{m}$ by a Pb collimator with two cross-slices. A monochromatic X-ray with photon energy of 16.5 keV was used to excite the samples. Samples were mounted on XYZ translation stages and the sample platform was moved by a 2D stepping motor along the X directions

of $40 \text{ }\mu\text{m}$ and Z directions of $60 \text{ }\mu\text{m}$ for each step. A light microscope was coupled to a computer for sample observation.

Three of the exposed and control samples were analyzed by SR- μXRF , respectively. The bio-mapping of Fe in the olfactory bulb and brain regions was obtained by means of the normalization to Compton scattering intensity to correct the difference of thickness between various regions of the brain section (Wang et al., 2010).

2.4. Immunofluorescence microscopy for microglial activation

Under deep anesthesia with sodium pentobarbital (80 mg/kg body weight), the animals ($n=3$ to each group) were perfused through the left cardiac ventricle with physiological saline followed by ice-cold fixative which consist of 4% paraformaldehyde in 0.1 mol/L phosphate buffer (PB, pH 7.4). After perfusion, the brain was quickly removed, postfixed at 4°C for 4 h in the same fixative, and then cryoprotected overnight in 0.1 mol/L PB buffer containing 30% sucrose, pH 7.4. Frozen brains were coronally cut into $20\text{-}\mu\text{m}$ -thick sections on a freezing microtome (Reichert–Jung, Heidelberg, Germany).

For immunofluorescence microscopic observation of microglia, the cryostat brain sections ($n=3$) were permeabilized with 0.3% Triton X-100 in 0.01 mol/L phosphate buffered saline (PBS, pH 7.4) for 15 min, and then immersed in 3% hydrogen peroxide in methanol to block endogenous peroxidase for 20 min followed by three PBS washes. After that, sections were placed with 5% bovine serum albumin (BSA) in PBS for 60 min at room temperature, then incubated in a moist-air

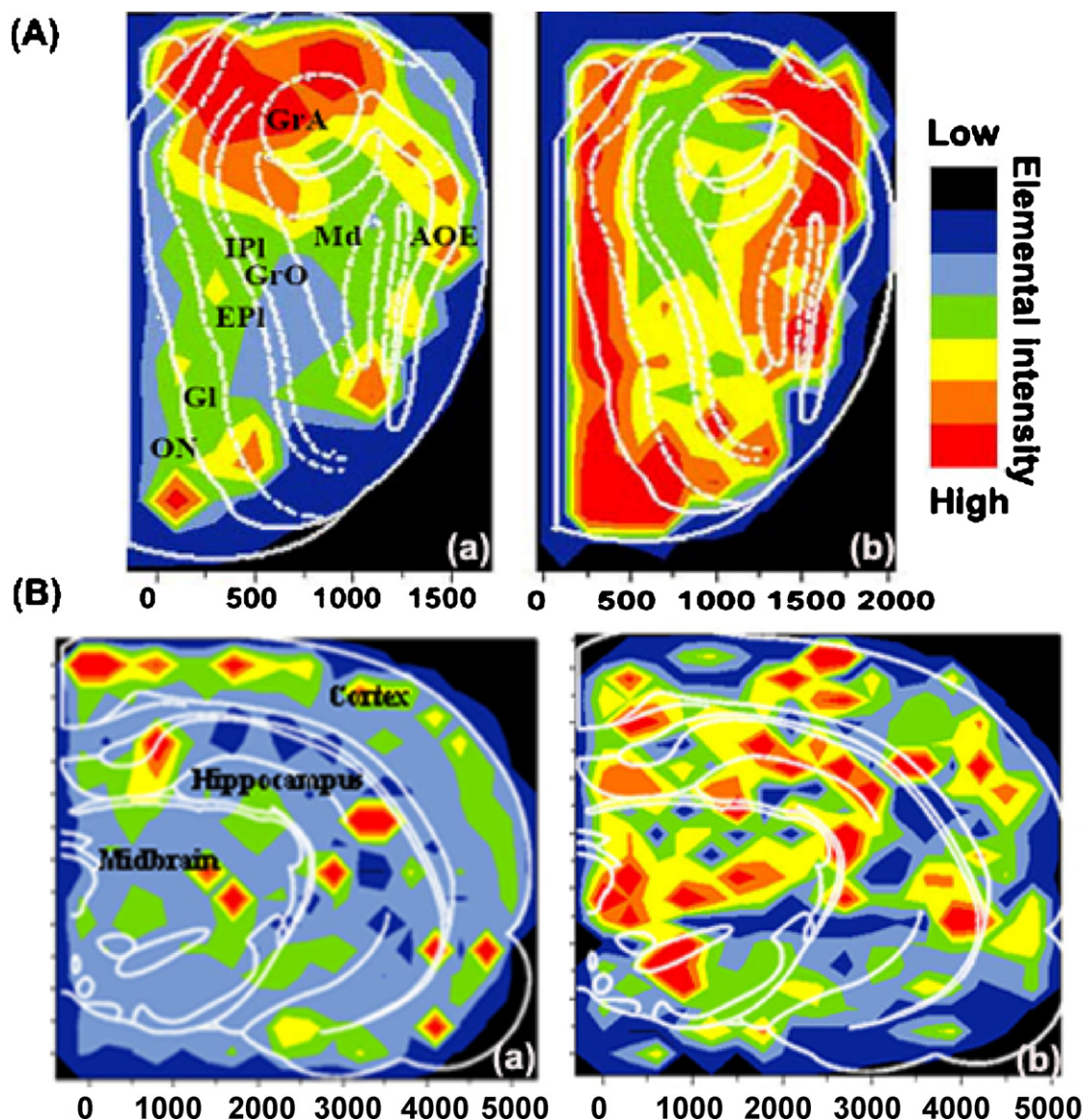


Fig. 1. Fe distribution in mouse olfactory bulb (A) and brain regions (B) tested by SR- μXRF . (a) Control group, (b) Fe_2O_3 -NP group. ON: olfactory nerve layer, GI: glomerular layer, Epl: external plexiform layer, Ipl: internal plexiform layer, GrO: granule cell layer of olfactory bulb, Md: medullary layer, GrA: granule cell layer of accessory olfactory bulb, AOE: anterior olfactory nucleus external part.

chamber overnight at 4 °C with rat anti-mouse CD11b (1:100 dilution, Mac1 α , BD Pharmingen). After washing in PBS, the sections were incubated with FITC-labeled goat anti-rat IgG (1:200 dilution, Kirkegaard & Perry Laboratories Inc., USA) for 2 h. Finally, sections were rinsed and mounted with 30% glycerol in PBS. The immunohistochemical staining was observed under Confocal microscopy (PerkinElmer Inc., USA).

For Nissl staining, brain sections were mounted directly onto gelatin-coated glass slides and air-dried. The slides were stained with 0.5% cresyl violet, dehydrated and delipidated in xylene, and cover-slipped with Entellan (Merck, Germany).

2.5. Cell culture and exposure to nanoparticles

The immortalized murine microglial cell line BV2 was purchased from the Cell Culture Center, Institute of Basic Medical Sciences, Chinese Academy of Medical Sciences. The cells were grown in Dulbecco's Modified Eagle Medium (DMEM, Gibco) containing 10% fetal calf serum (FCS, TBD Science, Tianjing, China), 100 U/mL penicillin and 100 μ g/mL streptomycin (North China pharmaceutical Group Corp., Hebei, China), and maintained at 37 °C in a humidified atmosphere with 5% CO₂. After reaching 80% confluence, the cells were digested by 0.25% pancreatin (Amresco Inc., Solon, OH, USA) and seeded to 96-well plates at a density of 1×10^4 cells per well or 6-well plates with 2×10^5 cells per well. After a 24 h cultivation period, medium

was replaced by fresh medium which contained 0.02, 0.2, 2 mol Fe/L of Fe₂O₃-NP suspensions or FeCl₃ solution. The FeCl₃ (Beijing Chemistry Corp., China) was used as the iron ion control with the same Fe concentration in the Fe₂O₃-NP suspension.

2.6. TEM observation

For TEM observation, the BV2 cells were cultured in 6-well plates and exposed to Fe₂O₃ NPs at final Fe concentration of 0.2 mmol/L for 6 h. After exposure, cells were washed in warm PBS to remove all non-internalized particles and digested by 0.25% pancreatin. Then the BV2 cells were collected and washed with PBS. After that, the cells were fixed in 2.5% glutaraldehyde (pH 7.4) overnight and the samples were treated according to the general protocols for TEM study. The ultra-thin sections (70–100 nm) were stained with lead citrate and uranyl acetate. The specimens were examined using JEOL electron microscopy (JEM-100CX II).

2.7. Cell viability assay

The effects on cell viability after the treatments with different concentrations of Fe₂O₃ NPs were evaluated by using Cell Counting Kit-8 assay (CCK-8, Dojindo Laboratories, Kumamoto, Japan). The CCK-8 assay is based on the measurement of the amount of the formazan generated by the activity of dehydrogenases bioreducing

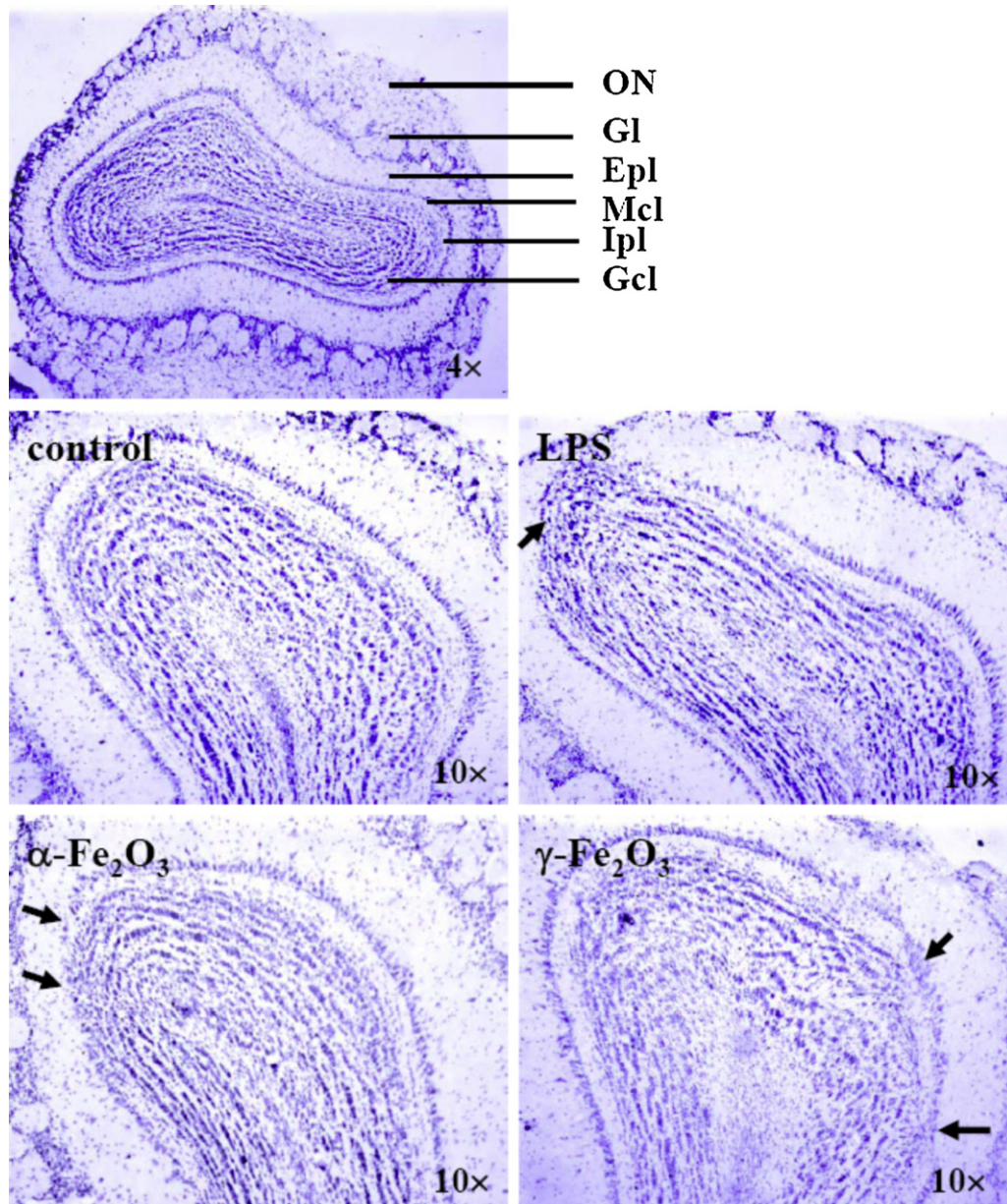


Fig. 2. Nissl stained coronal section of mouse olfactory bulb. Compared with control group, the exposed group (LPS, α -Fe₂O₃ and γ -Fe₂O₃ NPs) showed significant pathological changes in mouse olfactory bulb, especially on the MCL, IPL and GCL. Arrows show irregular arrangement of neuron cells. Objectives: 4 \times , 10 \times . ON: olfactory nerve layer, Gl: glomerular layer, Epl: external plexiform layer, Mcl: mitral cell layer, Ipl: internal plexiform layer, Gcl: granule cell layer.

of WST-8 (2-(2-methoxy-4-nitrophenyl)-3-(4-nitrophenyl)-5-(2,4-disulphophenyl)-2H-tetrazolium, monosodium salt) in cells, which is directly proportional to the numbers of living cells. The cells in 96-well plate were incubated with WST-8 for 1 h. Then the supernatants were collected and centrifuged to remove the exposed nanoparticles. The absorbance of formazan was measured at 450 nm against a reference wavelength of 650 nm using a microplate reader (SpectraMax M2, Molecular Devices Corp., USA). The use of dual wavelength analysis can provide better precision because the reference wavelength may selected for cancellation of the signal alteration caused by NPs.

2.8. ROS assay

The generation of intracellular ROS was measured by the DCFH-DA reagent (Beyotime Institute of Biotechnology, Jiangsu, China). Cells were incubated in serum-free DMEM containing 10 $\mu\text{g}/\text{mL}$ DCFH-DA at 37 °C for 30 min. After washing cells by PBS for three times, cells were treated with Fe_2O_3 NPs from 15 min to 12 h. DCFH-DA can enter cell passively and can be hydrolyzed by esterases to nonfluorescent DCFH. When the DCFH is oxidized by ROS, it is transformed to the highly fluorescent 2',7'-dichlorofluorescein (DCF). The fluorescence of DCF was monitored at 488 nm for excitation wavelength and 525 nm for emission wavelength using a fluorescence microplate reader (SpectraMax M2, Molecular Devices Corp., USA). The 3-morpholino-sydnonimine hydrochloride (SIN-1) was employed as a positive control. Cell free experiments with and without NPs

were conducted to control the interference of fluorescence measurement from NPs.

2.9. Nitric oxide assay

Nitric oxide (NO) content was detected by the amount of nitrite accumulated in culture supernatant using Griess Reagent (Beyotime Institute of Biotechnology, Jiangsu, China). Cells were planted in 96-well plates and exposed to NPs from 2 h to 24 h. The culture supernatant was collected and centrifuged to remove the NPs. In 96-well plates, 50 μL Griess reagent and 50 μL culture supernatant were mixed. The absorbance was measured at 540 nm. The nitrite concentration was calculated from a sodium nitrite standard curve.

2.10. Cytokine assay

Cells were planted in 96-well plates and exposed to NPs for 6 h. The culture supernatants were collected and centrifuged to remove the NPs. The concentrations of cytokines (IL-1 β , IL-6, TNF- α) in supernatants were measured by enzyme-linked immunosorbent assay (ELISA) kits (specific for mice, 4A biotech Co. Ltd., China) according to the manufacturer's instructions. Cytokine concentrations were calculated with the standard curves generated from fixed amounts of mouse recombinants IL-1 β , IL-6 and TNF- α . Photometric measurements were conducted at

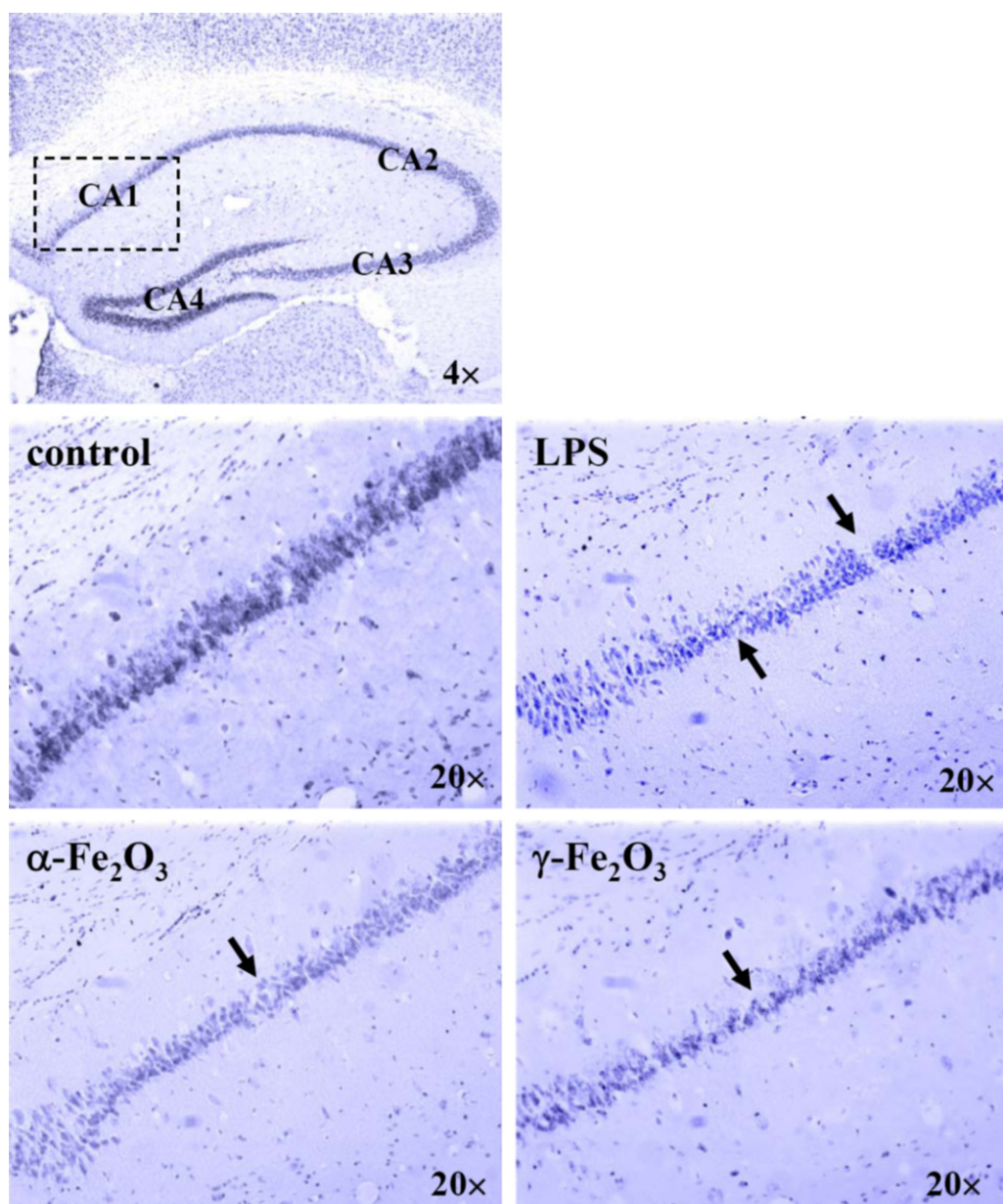


Fig. 3. Nissl stained coronal section of mouse hippocampus CA1 region. Arrows show the thin cell layer and loose-arranged pyramidal cells. Objectives: 4 \times , 20 \times .

450 nm using a microplate reader. The detection limits for the cytokine assays were as follows: IL-1 β , 4 pg/mL; IL-6, 4 pg/mL; TNF- α , 15 pg/mL.

2.11. Statistical analysis

Data were expressed as means \pm SD and analyzed with SPSS 12.0. Independent-samples *t*-test was used to assess the significant difference between two experimental groups. One-way variance (ANOVA) with LSD or Games-Howell tests was applied to evaluate the statistical significance of differences between the experimental groups and the controls. A *p* value less than 0.05 was considered to be statistically significant.

3. Results

3.1. Physicochemical properties of Fe₂O₃ nanoparticles

The physicochemical properties of two kinds of Fe₂O₃ NPs are shown in Table 1. The α -Fe₂O₃ NPs are widely used in pigments, sensors, catalysts and wastewater treatment (Chen et al., 2005; Zhong et al., 2006). The γ -Fe₂O₃ NPs because of its superparamagnetic property show promise applications in magnetic storage media and biomedicine, such as MRI contrast agent, targeted drug delivery and so forth (Berry and Curtis, 2003). As shown in Table 1, the α -Fe₂O₃ NPs has a corundum structure with an average size of 22 ± 5 nm, while, the γ -Fe₂O₃ NPs has a defect spinel crystal structure and the average size is 31 ± 17 nm. The BET specific surface areas of the γ -Fe₂O₃ NPs (33.2 m²/g) were three times larger than the α -Fe₂O₃ ones (11.2 m²/g).

In aqueous dispersion conditions, including PBS and cell culture medium (DMEM with or without serum), the iron oxide NPs aggregated into larger particles (Table 1). Comparatively, the NPs

have the smallest average hydrodynamic sizes in DMEM containing 10% FCS, meanwhile, the α -Fe₂O₃ NPs present much smaller size than the γ -Fe₂O₃ ones. The data of zeta potentials showed that the α -Fe₂O₃ NPs were more stable in cell culture than the γ -Fe₂O₃ NPs.

3.2. Elemental mapping of Fe in olfactory bulb and brain regions after Fe₂O₃ nanoparticle exposure

The micro-distribution mapping of Fe by SR- μ XRF analysis clearly showed that the concentrations of Fe obviously elevated in olfactory nerve layer (ON), glomerular layer (Gl), external plexiform layer (Epl), internal plexiform layer (Ipl), and anterior olfactory nucleus external part (AOE) of olfactory bulb of the NP-exposed mice comparing with the untreated mice (Fig. 1). In other brain regions, Fe levels significantly increased in cortex, hippocampus, and midbrain compartments after NP exposure (Fig. 1).

3.3. Neuropathological changes in mouse brain

Nissl staining showed some morphological changes in mouse brain after LPS and NP treatments. The irregular arrangement of neuron cells or neuronal loss in olfactory bulb, especially in the mitral cell layer (Mcl), internal plexiform layer (Ipl) and granule cell layer (Gcl) were found (Fig. 2). Obviously, part of the mitral cell layer (Mcl) and internal plexiform layer (Ipl) disappeared in the NP-treated mice.

In deep brain regions, such as hippocampus and striatum, some neuropathological changes were observed as well (Figs. 3 and 4). In the CA1 region of normal mouse hippocampus, the pyramidal

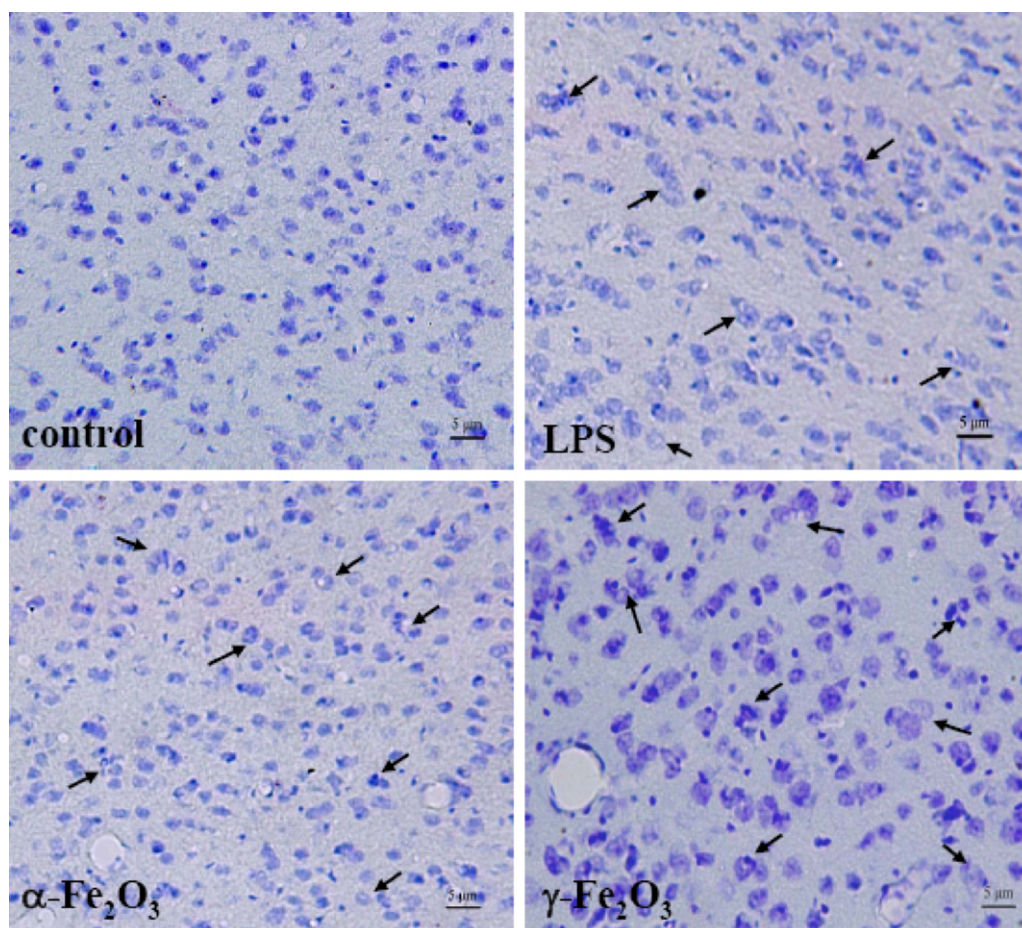


Fig. 4. Nissl stained coronal section of mouse striatum. Arrows show cellular swelling, vacuolar degeneration, nucleus concentration or fragment. Objectives: 40 \times .

cells are regularly and closely arranged and form multilayer structure. However, after exposure to LPS, α -Fe₂O₃ and γ -Fe₂O₃ NPs, the number of intact neuronal cells in the hippocampal CA1 was significantly decreased, and the pyramidal cells arranged loosely, presenting obviously thinner layer than in the normal mice (Fig. 3). In striatum of the exposed mice (LPS, α -Fe₂O₃ and γ -Fe₂O₃ NP groups), the neuropathological changes displayed cellular swelling, vacuolar degeneration, nuclear chromatin condensation and fragmentation (Fig. 4). Similarly pathological changes in cerebral cortex of the exposed groups were found as well (Supplemental Data, Fig. S1). No apparent differences were observed in substantia nigra between exposed and normal mice.

3.4. Fe₂O₃ nanoparticle intranasal exposure induced microglial activation in mouse brain

Activated microglia were visualized via immunofluorescence microscopy with antibody against the CD11b antigen (Sugama et al., 2007). In the study, the immunofluorescent images clearly exhibited increased numbers of activated microglia in olfactory bulb of the LPS and the two Fe₂O₃-NP group mice (Fig. 5). In the control mice, microglia showed “resting face” with a small cell body in the fine, ramified processes, nevertheless, in the positive LPS and NP group mice, microglia showed “activated face” though still ramified but with stouter cell processes (Fig. 5, top-right). The LPS group showed a diffuse presence of activated microglial cells in all the layers of the olfactory bulb, nevertheless, the α -Fe₂O₃-NP and γ -Fe₂O₃-NP groups displayed the microglial proliferation and activation mainly in the olfactory nerve layer (ON) and glomerular

layer (GL). The γ -Fe₂O₃ NPs were likely to induce more significant proliferation of activated microglia than the α -Fe₂O₃ NPs did.

The increase in the numbers of activated microglia was also observed in the hippocampus, from CA1 to CA4 regions, and in the striatum of the exposed groups (LPS, α -Fe₂O₃ and γ -Fe₂O₃ NP groups, Figs. 6 and 7). In cerebral cortex, similar results as in striatum were found as well (Supplemental Data, Fig. S2). No apparent differences were observed in substantia nigra between exposed and normal mice.

3.5. Fe₂O₃ nanoparticle exposure induced microglial cells proliferation, activation and release of ROS and NO

Experiments with BV2 cells showed the Fe₂O₃ NPs exposure had no significant cytotoxic effects (Fig. 8). Comparing with the results of α -Fe₂O₃-NP, the γ -Fe₂O₃-NP treatment is likely to promote cell viability. The iron ion could induce significant dose-dependent decrease effect on the viability of BV2 cells, however, with the exposed time lasted to 12 h, the viability of cells recovered to the normal level.

Further analysis showed the exposure of BV2 microglial cells to the Fe₂O₃ NPs induced significant cell excretion of ROS and NO (Fig. 9A and B). The NO content obviously increased at the early exposed-time point (Fig. 9B). The iron ions caused the highest ROS and NO levels, which may be associated with the Fenton's reaction. However, no significantly elevated levels of inflammatory cytokines, including IL-1 β , IL-6 and TNF- α , were found by Fe₂O₃ NP treatment (Fig. 10).

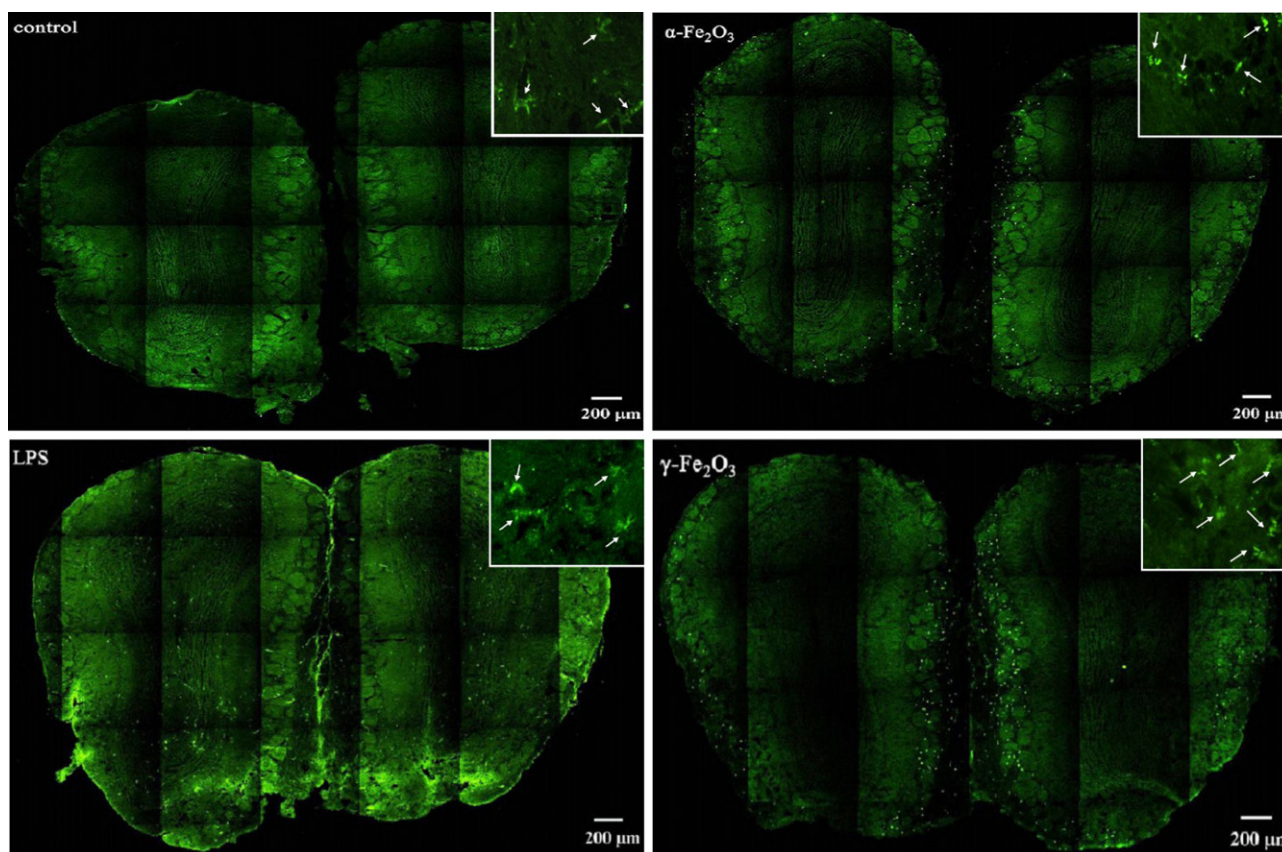


Fig. 5. Immunofluorescence staining of CD11b in mouse olfactory bulb. Arrows in the box on the top right corner show CD11b-immunoreactive microglia (Objectives: 40 \times). The exposed groups (LPS, α -Fe₂O₃ and γ -Fe₂O₃ NPs) have significantly increased numbers of activated microglia in mouse olfactory bulb. The LPS exposure group showed a diffuse distribution of microglial cells. The α -Fe₂O₃ and γ -Fe₂O₃ NPs induced microglial proliferation and activation mainly concentrated in the olfactory nerve layer (ON) and glomerular layer (GL). Figures on top-right show the microglia presenting “resting face” with a small cell body in the fine, ramified processes in control mice; in the positive LPS and NP group mice, microglia present “activated face” with stouter cell processes.

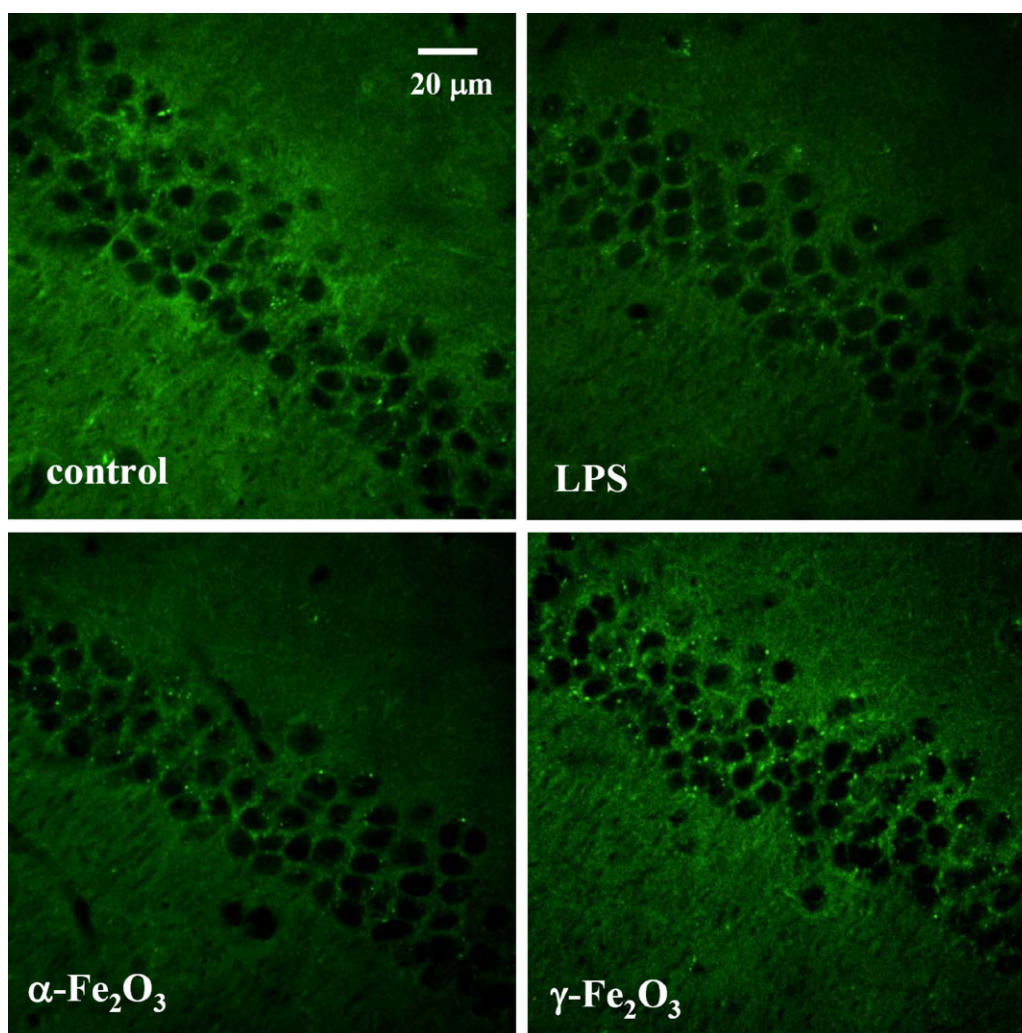


Fig. 6. Immunofluorescence staining of CD11b in mouse hippocampus. The increased numbers of activated microglia were observed in the exposed groups. (LPS, α - Fe_2O_3 and γ - Fe_2O_3 NPs.)

3.6. Phagocytosis of Fe_2O_3 nanoparticles by microglia

Microglia are the resident macrophage-like cells in the brain and act as the first line of defense against microorganism invasion and injury. After BV2 cells exposure to the Fe_2O_3 NPs for 6 h, the TEM images clearly showed that some particles were phagocytized by the cells (Fig. 11). The exposure induced a large number of cellular vesicles, accompanying proliferation of lysosome, swelling of endoplasmic reticulum and disappearance of mitochondrial cristae in the BV2 microglial cells.

4. Discussion

The responses and functions of microglia in the processes of CNS lesion have been ignored for a quite long time, but in the last 20 years the microglia field has developed into a very active branch of neuroscience. Up to now, microglial cells function is confirmed as guardians of the brain and spinal cord, acting not only as a tissue alarm system but also exerting defense, as well as repair functions of nerve cells (Graeber, 2010). It has been found that the activation of microglia may respond sensitively to even minor pathological challenges that affect the CNS, though the exact profile of the microglia has not yet been well known (Hanisch and Kettenmann, 2007).

As for the case of nanoparticles, several epidemiological investigations have found that particulate matters, which is now known as the component of ultrafine particles (diameter < 100 nm), are implicated in the aetiology of some neurodegenerative diseases, such as ischaemic stroke and Parkinson's disease (Elbaz et al., 2004; Wellenius et al., 2005). Increasing evidence indicates that the possible mechanisms may include particles-induced inflammation and microglial activation in brain. For example, some environmental toxins, such as heavy metals, pesticides, infectious agents and so forth are implicated in the development and progression of the Parkinson's disease. One of the possible mechanisms is the cumulative influence of environmental insults on microglia activation promotes the development of the disease (Elbaz et al., 2004). Nanoparticles, with much similar properties of ultrafine particulate matter, have ultrahigh biological and chemical activities, facily induce numerous inflammations in organisms and easily transport into systemic circulation, thus, receive increasing attention to their safety on human health. The environmental studies offer a valuable insight into the potential risk of nanoparticles to neurological deterioration. However, little is known about the microglia respond to nanoparticles in brain.

So far, nanoparticles have been demonstrated to be efficiently deposited in nasal, tracheobronchial and alveolar regions by diffusion when inhaled exposure (Oberdörster et al., 2005). Ours and many other pervious studies reported that deposited nanoparticles

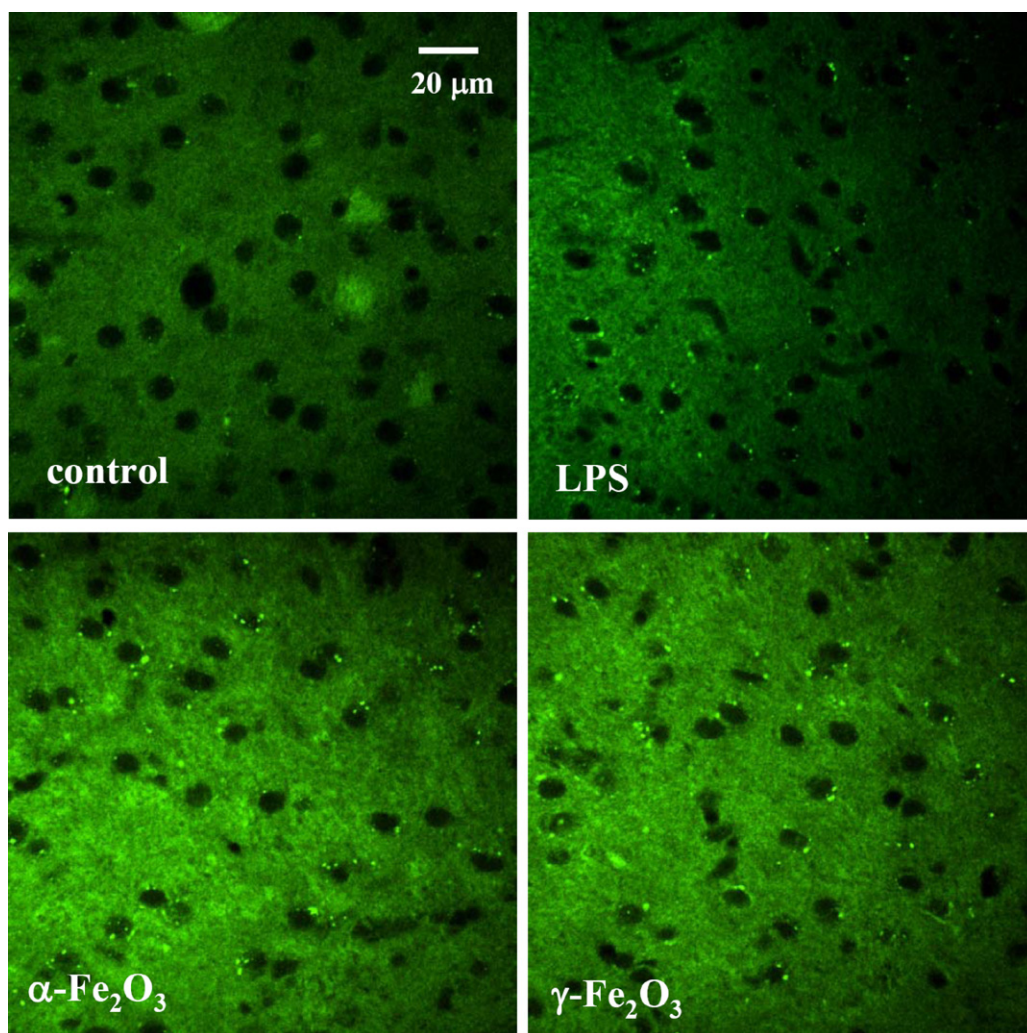


Fig. 7. Immunofluorescence staining of CD11b in mouse striatum. The increased numbers of activated microglia were observed in the exposed groups. (LPS, α-Fe₂O₃ and γ-Fe₂O₃ NPs.)

in olfactory mucosa of the nasal region may transport along the olfactory nerve into the olfactory bulb and are capable of inducing brain pathological damage (Wang et al., 2008a, 2009; Tin-Tin-Win-Shwe et al., 2008; Elder et al., 2006). These results indicated that the olfactory bulb of the brain was targeted by inhaled nanoparticles. In the present study, we have systemically examined the recruitment of microglial cells in the nanoparticle transport pathway in olfactory bulb and the related brain regions, and compared

with the results of neuropathological alteration after the mice intranasal exposure to Fe₂O₃ NPs for 40 days. The pathological alteration was found in olfactory bulb, hippocampus, and slightly changes in striatum and cerebral cortex. Comparatively, the most significantly pathological changes were found in olfactory bulb. The immunofluorescence microscopy allows directly visualize the activated microglia in brain section. In the study, we observed the activated microglial cells in olfactory bulb, hippocampus and

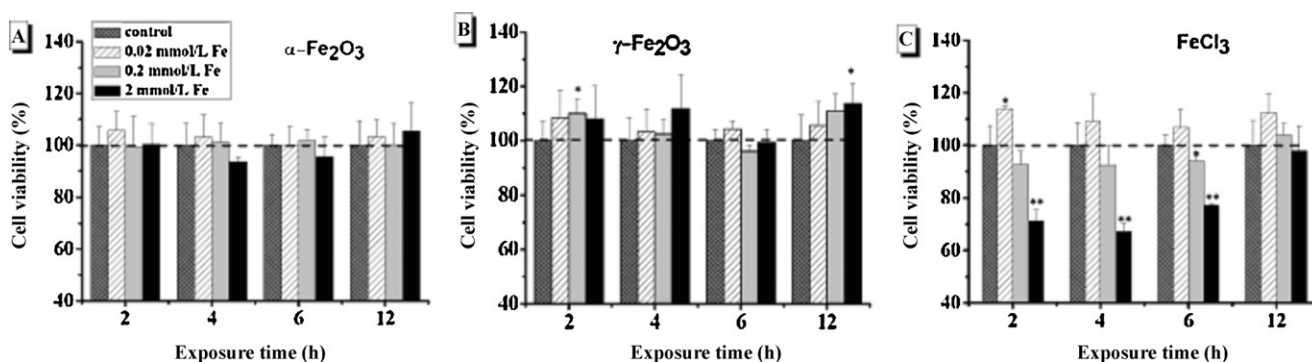


Fig. 8. Effect of iron oxide nanoparticles on the viabilities of microglia. BV2 microglial cells were treated with α-Fe₂O₃ NPs (A), γ-Fe₂O₃ NPs (B) and FeCl₃ (C) for 2 h, 4 h, 6 h and 12 h. The data presents as mean ± SD (n = 3). Significant difference from the control. *p < 0.05 or **p < 0.01.

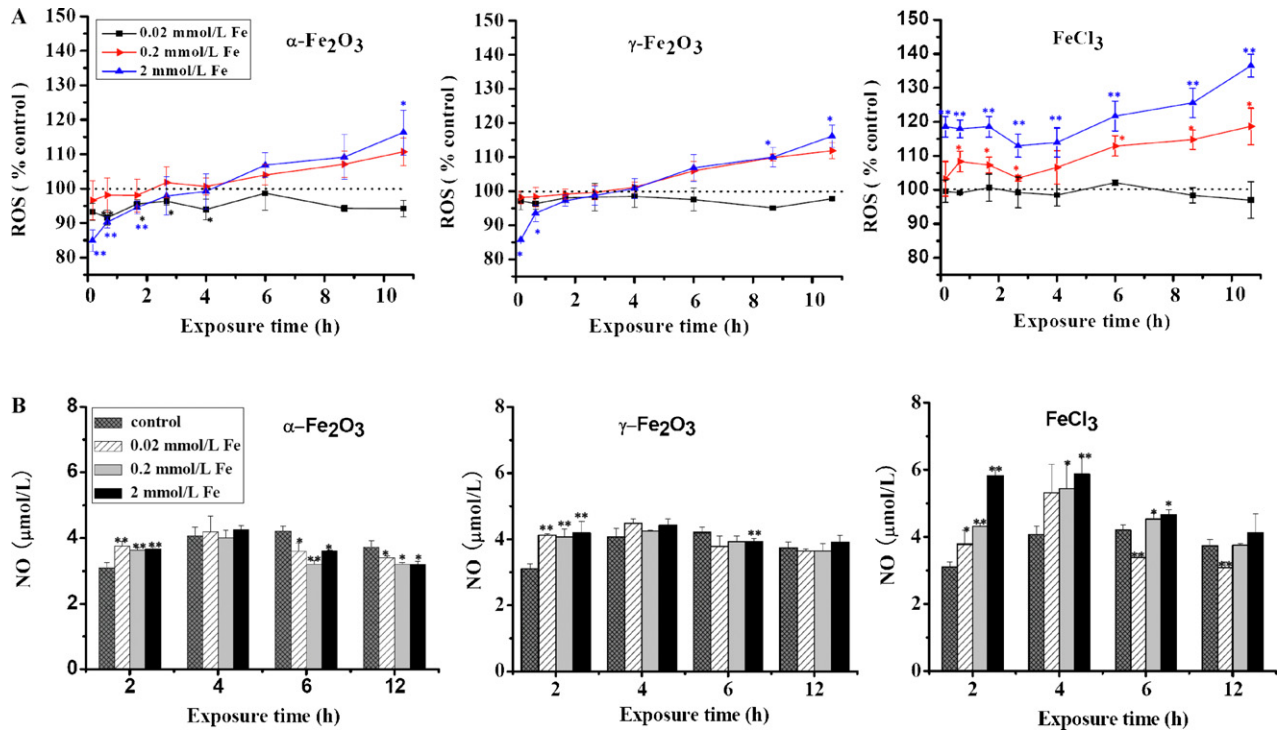


Fig. 9. The production of reactive oxygen species (ROS, for 0–10 h treatment, A) and nitric oxygen (NO, for 2 h, 4 h, 6 h and 12 h treatment, B) in microglia after exposure to iron oxide NPs. BV2 microglial cells were treated with α-Fe₂O₃ NPs, γ-Fe₂O₃ NPs and FeCl₃ for 0–10 h. The data presents as mean ± SD (n = 3). Significant difference from the control, *p < 0.05 or **p < 0.01.

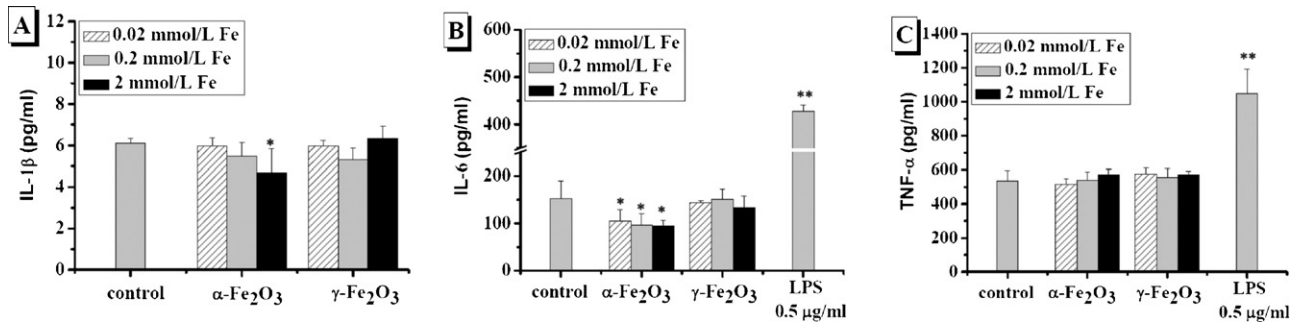


Fig. 10. The protein levels of cytokines IL-1 beta, IL-6 and TNF-alpha in microglia after exposure to iron oxide NPs. BV2 microglial cells were treated with α-Fe₂O₃ NPs (A), γ-Fe₂O₃ NPs (B) and FeCl₃ (C) for 6 h. The data presents as mean ± SD (n = 3). Significant difference from the control, *p < 0.05 or **p < 0.01.

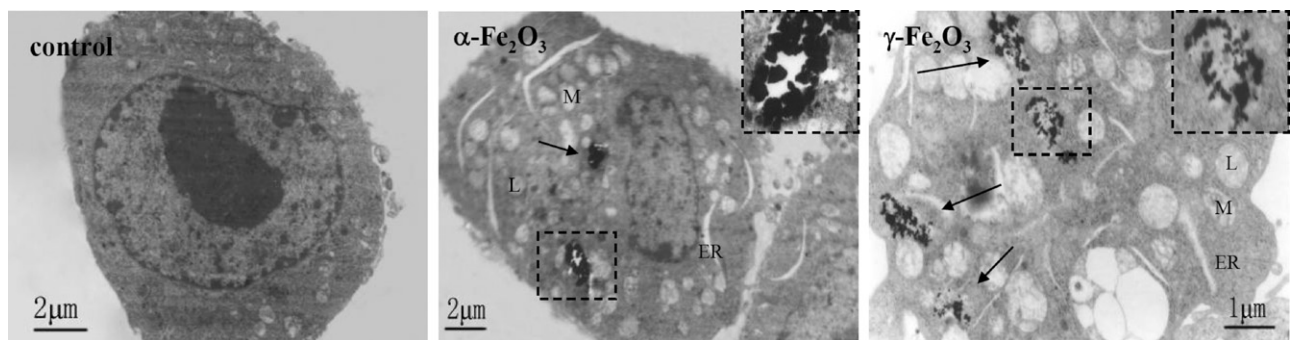


Fig. 11. TEM images of microglia. BV2 microglial cells were treated with 0.2 mmol/L Fe content of α-Fe₂O₃ or γ-Fe₂O₃ NPs for 6 h. The NPs were phagocytized into microglial cells and localized in vesicles. The arrow indicates particle aggregates. The cellular ultrastructure was seriously damaged. M: mitochondrion, L: lysosome, ER: endoplasmic reticulum.

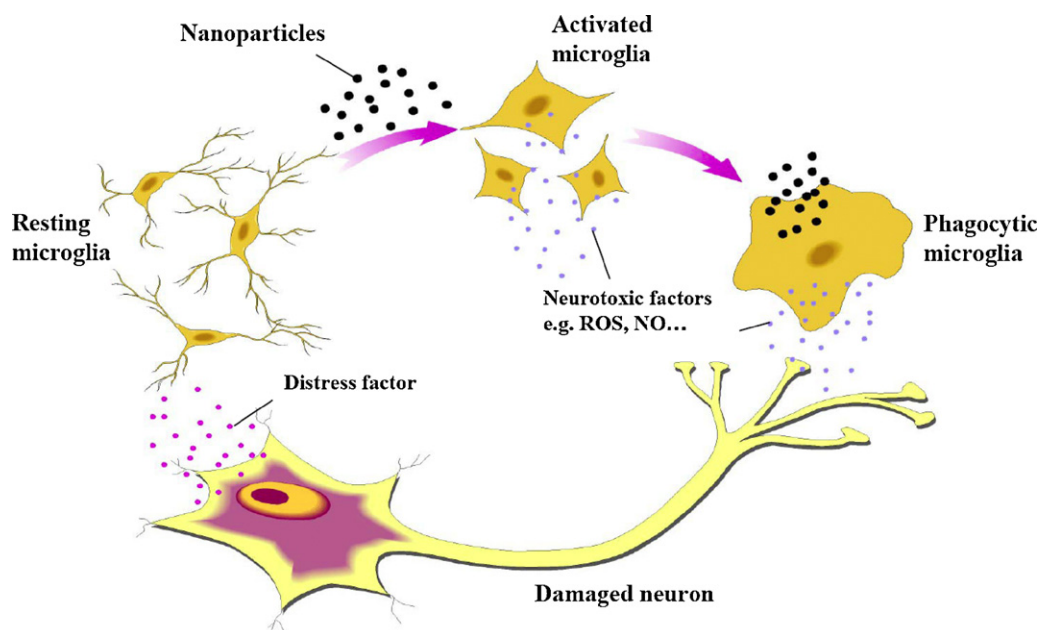


Fig. 12. The mediation role of microglia for the protection or neurotoxicity of brain after intranasal exposure of Fe_2O_3 NPs.

striatum, accordingly with the storage route of Fe_2O_3 NP shown by SR- μ XRF images and the alteration regions of the pathological reports. The most number of activated microglia were found in the olfactory nerve layer (ON) and glomerular layer (GL), which was consistent with the transport pathway of Fe_2O_3 NPs along the olfactory nerve layers.

We concern on if the activated microglia may release some cytotoxic factors such as ROS, NO and inflammatory cytokines that might cause neurotoxicity in response to the nanoparticle transportation. The murine BV2 cell line is immortalized by infecting primary microglial cell cultures with a v-raf/v-myc recombinant retrovirus that can exhibit the phenotypic and functional properties of reactive microglial cells (Blasi et al., 1990; Bocchini et al., 1992). As a model of microglial cells, BV2 cells have been widely used in neuroscience research. The responses of BV2 cells to the exposure of Fe_2O_3 NPs may have implications for the reactions of particles in CNS. Here we found the exposure of BV2 to Fe_2O_3 NPs induced the cell proliferation, phagocytosis, and the release of ROS and NO, which were all the typical parameters for enhanced microglia activation. However, no significantly elevated levels of inflammatory cytokines, including IL-1 β , IL-6 and TNF- α , have been observed.

Accumulating evidence strongly suggested that ROS generation and the induction of oxidative stress is a major toxicological paradigm for engineered nanoparticles (Donaldson and Stone, 2003; Meng et al., 2009; Nel et al., 2006; Rahman et al., 2009). In our previous work, we observed that the intranasal exposure of Fe_2O_3 NPs induced significant oxidative stress responses in mouse olfactory bulb and hippocampus (Wang et al., 2009). The ROS has been proposed to play a pathogenic role in neuronal injury, whereas, the microglia play an active role in mediation of the oxidative damage (Block et al., 2004; Long et al., 2007). It was found that diesel exhaust particles (DEP) selectively damaged dopaminergic neurons through the phagocytic activation of microglial NADPH oxidase and consequent oxidative-insult (Block et al., 2004). The titanium dioxide NPs were observed to rapidly damage neurons at low concentrations in complex brain cultures, plausibly through microglial generated ROS (Long et al., 2007).

It is known that nitric oxide (NO) has an array of functions in the CNS, such as the regulation of synaptic plasticity, the sleep-wake cycle and hormone secretion, apart from the above mentioned

physiological functions, NO becomes noxious if it is produced in excess (Calabrese et al., 2007; Pacher et al., 2007). Cell pro-oxidant state can promote NO to undergo oxidation–reduction reactions and to form peroxynitrite (ONOO^-) and other reactive nitrogen species (RNS), which lead to nitrosative stress and cellular damage (Calabrese et al., 2007; Pacher et al., 2007).

Collectively, the results from the *in vivo* and *in vitro* investigations all show that the intranasal exposure of Fe_2O_3 NPs may induce microglia activation, recruitment and phagocytosis in brain. Once Fe_2O_3 NPs store in brain and cause neuron injury, the surrounding microglia may quickly recruit to the lesion sites and activate readily that play an active role in host defense and repair in the CNS; however, the excessed activated microglia may produce free radicals (ROS and NO) that damage neighbouring neurons, resulting in a perpetuating cycle of neuron death. Several studies have revealed that the damaged neurons can also release several factors, such as matrix metalloproteinase-3 (MMP-3), α -synuclein, neuromelanin and ATP that conversely to activate microglia (Block et al., 2007; Honda et al., 2001; Kim et al., 2005). The mediation role of microglia for the protection or neurotoxicity of brain after Fe_2O_3 NP intranasal exposure is described in Fig. 12. We conclude that the microglial may play an active role in the process of the exogenous Fe_2O_3 NP invading and storage in brain.

Additionally, the current results in both animal and cell experiments show some evidence that the γ - Fe_2O_3 NPs could induce more serious pathological damages in animal brain, evoke more significant microglial proliferation and activation, and release higher levels of ROS and NO in microglial cells than the α - Fe_2O_3 -NP did. These phenomena could be explained by the high surface activities of γ - Fe_2O_3 NPs, because γ - Fe_2O_3 NPs possess high specific surface area due to their defected crystal structure.

In summary, our results provide the first systematic mapping of activated microglia in the brain areas of mice by nanoparticle intranasal exposure. We show that the intranasal exposure of ferric oxide NPs may lead to brain pathological alteration, microglial proliferation, activation and recruitment, especially in olfactory regions. Experiments with microglial cells indicate that the activated microglia can phagocytize nanoparticles, and generate significantly elevated levels of ROS and NO. We conclude the microglial activation may act as an alarm and defense system in the

process of the exogenous NP invading and storage in brain. However, because of the two-edge functions of microglia in CNS, the exact understanding of whether microglia would be neuroprotective or neurotoxic and what promotes transformation between the two functions need further study.

Conflict of interest statement

The authors declare that there are no conflicts of interest.

Acknowledgements

National Basic Research Program of China (2011CB933403), the Chinese Academy of Sciences (KJXC3.SYWN3) and the National Natural Science Foundation of China (10975148 and 10905064).

Appendix A. Supplementary data

Supplementary data associated with this article can be found, in the online version, at doi:10.1016/j.toxlet.2011.05.001.

References

- Berry, C., Curtis, A., 2003. Functionalisation of magnetic nanoparticles for applications in biomedicine. *J. Phys. D: Appl. Phys.* 36, R198.
- Blasi, E., Barluzzi, R., Bocchini, V., Mazzolla, R., Bistoni, F., 1990. Immobilization of murine microglial cells by a V-Raf/V-Myc carrying retrovirus. *J. Neuroimmunol.* 27, 229–237.
- Block, M.L., Wu, X., Pei, Z., Li, G., Wang, T., Qin, L., Wilson, B., Yang, J., Hong, J.S., Veronesi, B., 2004. Nanometer size diesel exhaust particles are selectively toxic to dopaminergic neurons: the role of microglia, phagocytosis, and NADPH oxidase. *FASEB J.* 18, 1618–1620.
- Block, M.L., Zecca, L., Hong, J.S., 2007. Microglia-mediated neurotoxicity: uncovering the molecular mechanisms. *Nat. Rev. Neurosci.* 8, 57–69.
- Bocchini, V., Mazzolla, R., Barluzzi, R., Blasi, E., Sick, P., Kettenmann, H., 1992. An immortalized cell-line expresses properties of activated microglial cells. *J. Neurosci. Res.* 31, 616–621.
- Calabrese, V., Mancuso, C., Calvani, M., Rizzarelli, E., Butterfield, D.A., Stella, A.M., 2007. Nitric oxide in the central nervous system: neuroprotection versus neurotoxicity. *Nat. Rev. Neurosci.* 8, 766–775.
- Chen, J., Xu, L., Li, W., Gou, X., 2005. α -Fe₂O₃ nanotubes in gas sensor and lithium-ion battery applications. *Adv. Mater.* 17, 582–586.
- De Lorenzo, A., Darin, J., 1970. The olfactory neuron and the blood-brain barrier. In: Wolstenholme, G.E.W., Knight, J. (Eds.), *Taste and Smell in Vertebrates*. J&A Churchill, London, pp. 151–176.
- Donaldson, K., Stone, V., 2003. Current hypotheses on the mechanisms of toxicity of ultrafine particles. *Ann. Ist. Super. Sanita.* 39, 405–410.
- Elbaz, A., Levecque, C., Clavel, J., Vidal, J., Richard, F., Amouyel, P., Alperovitch, A., Chartier-Harlin, M., Tzourio, C., 2004. CYP2D6 polymorphism, pesticide exposure, and Parkinson's disease. *Ann. Neurol.* 55, 430–434.
- Elder, A., Gelein, R., Silva, V., Feikert, T., Opanashuk, L., Carter, J., Potter, R., Maynard, A., Ito, Y., Finkelstein, J., Oberdörster, G., 2006. Translocation of inhaled ultrafine manganese oxide particles to the central nervous system. *Environ. Health Perspect.* 114, 1172–1178.
- Graeber, M.B., 2010. Changing face of microglia. *Science* 330, 783–788.
- Hanisch, U.K., Kettenmann, H., 2007. Microglia: active sensor and versatile effector cells in the normal and pathologic brain. *Nat. Neurosci.* 10, 1387–1394.
- Honda, S., Sasaki, Y., Ohsawa, K., Imai, Y., Nakamura, Y., Inoue, K., Kohsaka, S., 2001. Extracellular ATP or ADP induce chemotaxis of cultured microglia through Gi/o-coupled P2Y receptors. *J. Neurosci.* 21, 1975–1982.
- Kim, Y.S., Kim, S.S., Cho, J.J., Choi, D.H., Hwang, O., Shin, D.H., Chun, H.S., Beal, M.F., Joh, T.H., 2005. Matrix metalloproteinase-3: a novel signaling proteinase from apoptotic neuronal cells that activates microglia. *J. Neurosci.* 25, 3701–3711.
- Kreyling, W.G., Semmler, M., Erbe, F., Mayer, P., Takenaka, S., Schulz, H., Oberdörster, G., Ziesenis, A., 2002. Translocation of ultrafine insoluble iridium particles from lung epithelium to extrapulmonary organs is size dependent but very low. *J. Toxicol. Environ. Health A* 65, 1513–1530.
- Lockman, P.R., Oyewumi, M.O., Koziara, J.M., Roder, K.E., Mumper, R.J., Allen, D.D., 2003. Brain uptake of thiamine-coated nanoparticles. *J. Control Release* 93, 271–282.
- Long, T.C., Tajuba, J., Sama, P., Saleh, N., Swartz, C., Parker, J., Hester, S., Lowry, G.V., Veronesi, B., 2007. Nanosize titanium dioxide stimulates reactive oxygen species in brain microglia and damages neurons in vitro. *Environ. Health Perspect.* 115, 1631–1637.
- Luo, X.G., Ding, J.Q., Chen, S.D., 2010. Microglia in the aging brain: relevance to neurodegeneration. *Mol. Neurodegen.* 5, 1–9.
- Meng, H., Xia, T., George, S., Nel, A.E., 2009. A predictive toxicological paradigm for the safety assessment of nanomaterials. *ACS Nano* 3, 1620–1627.
- Nel, A., Xia, T., Madler, L., Li, N., 2006. Toxic potential of materials at the nanolevel. *Science* 311, 622–627.
- Oberdörster, G., Oberdörster, E., Oberdörster, J., 2005. Nanotoxicology: an emerging discipline evolving from studies of ultrafine particles. *Environ. Health Perspect.* 113, 823–839.
- Oberdörster, G., Sharp, Z., Atudorei, V., Elder, A., Gelein, R., Kreyling, W., Cox, C., 2004. Translocation of inhaled ultrafine particles to the brain. *Inhal. Toxicol.* 16, 437–445.
- Occupational Safety and Health Administration (OSHA), 2003. Occupational Safety and Health Standards: Toxic and Hazardous Substances. Code of Federal Regulations, 29.
- Pacher, P., Beckman, J.S., Liaudet, L., 2007. Nitric oxide and peroxynitrite in health and disease. *Physiol. Rev.* 87, 315–424.
- Rahman, M.F., Wang, J., Patterson, T.A., Saini, U.T., Robinson, B.L., Newport, G.D., Muddock, R.C., Schlager, J.J., Hussain, S.M., Ali, S.F., 2009. Expression of genes related to oxidative stress in the mouse brain after exposure to silver-25 nanoparticles. *Toxicol. Lett.* 187, 15–21.
- Sharma, H.S., 2007. Nanoneuroscience: emerging concepts on nanoneurotoxicity and nanoneuroprotection. *Nanomed.* 2, 753–758.
- Stern, S.T., McNeil, S.E., 2008. Nanotechnology safety concerns revisited. *Toxicol. Sci.* 101, 4–21.
- Sugama, S., Fujita, M., Hashimoto, M., Conti, B., 2007. Stress induced morphological microglial activation in the rodent brain: involvement of interleukin-18. *Neuroscience* 146, 1388–1399.
- Suh, W.H., Suslick, K.S., Stucky, G.D., Suh, Y.H., 2009. Nanotechnology, nanotoxicology, and neuroscience. *Prog. Neurobiol.* 87, 133–170.
- Tin-Tin-Win-Shwe, Mitsushima, D., Yamamoto, S., Fukushima, A., Funabashi, T., Kobayashi, T., Fujimaki, H., 2008. Changes in neurotransmitter levels and proinflammatory cytokine mRNA expressions in the mice olfactory bulb following nanoparticle exposure. *Toxicol. Appl. Pharmacol.* 226, 192–198.
- Wang, B., Feng, W.Y., Wang, M., Shi, J.W., Zhang, F., Ouyang, H., Zhao, Y.L., Chai, Z.F., Huang, Y.Y., Xie, Y.N., Wang, H.F., Wang, J., 2007. Transport of intranasally instilled fine Fe₂O₃ particles into the brain: micro-distribution, chemical states, and histopathological observation. *Biol. Trace Elem. Res.* 118, 233–243.
- Wang, B., Feng, W.Y., Zhu, M.T., Wang, Y., Wang, M., Gu, Y.Q., Ouyang, H., Wang, H.J., Li, M., Zhao, Y.L., Chai, Z.F., Wang, H.F., 2009. Neurotoxicity of low-dose repeatedly intranasal instillation of nano- and submicron-sized ferric oxide particles in mice. *J. Nanopart. Res.* 11, 41–53.
- Wang, H., Wang, M., Wang, B., Meng, X.Y., Wang, Y., Feng, W.Y., Chai, Z.F., 2010. Quantitative imaging of element spatial distribution in the brain section of Alzheimer's disease mouse using synchrotron radiation X-ray fluorescence analysis. *J. Anal. Atom. Spectrom.* 25, 328–333.
- Wang, J., Chen, C., Liu, Y., Jiao, F., Li, W., Lao, F., Li, Y., Li, B., Ge, C., Zhou, G., Gao, Y., Zhao, Y., Chai, Z., 2008a. Potential neurological lesion after nasal instillation of TiO₂ nanoparticles in the anatase and rutile crystal phases. *Toxicol. Lett.* 183, 72–80.
- Wang, J., Liu, Y., Jiao, F., Lao, F., Li, W., Gu, Y., Li, Y., Ge, C., Zhou, G., Li, B., Zhao, Y., Chai, Z., Chen, C., 2008b. Time-dependent translocation and potential impairment on central nervous system by intranasally instilled TiO₂ nanoparticles. *Toxicology* 254, 82–90.
- Wellenius, G., Schwartz, J., Mittleman, M., 2005. Air pollution and hospital admissions for ischemic and hemorrhagic stroke among medicare beneficiaries. *Stroke* 36, 2549.
- Zhong, L., Hu, J., Liang, H., Cao, A., Song, W., Wan, L., 2006. Self-assembled 3D flower-like iron oxide nanostructures and their application in water treatment. *Adv. Mater.* 18, 2426–2431.